ELSEVIER

15 June 1997

Optics Communications 139 (1997) 11–16

OPTICS COMMUNICATIONS

Analysis of the irradiance along different paths in the image space using the Wigner distribution function

Genaro Saavedra, Walter D. Furlan, Enrique Silvestre, Enrique E. Sicre [1]

Departament d'Òptica, Universitat de València, E-46100 Burjassot (Valencia), Spain

Received 24 September 1996; revised 20 December 1996; accepted 19 February 1997

Abstract

The intensity distribution along different paths in the image space of an optical system is described in a two-dimensional phase-space domain in terms of the Wigner distribution function. This approach is useful for an efficient analysis of the performance of optical imaging systems suffering from spherical aberration. The good performance of the method is shown in some numerical simulations.

1. Introduction

There are several criteria for analyzing the performance of an optical imaging system when aberrations, focus errors and/or apodizer masks are present [1–3]. In most of these quality criteria, the on-axis image irradiance is the relevant quantity. However, as Hopkins has shown [4,5], some of these space approaches can be extended using the optical transfer function to give a tolerance criterion based on the spatial frequency behavior. More recently, several papers were published in which image quality parameters, like the Strehl ratio or the modulation transfer function, are studied using phase-space representations, mainly the Wigner distribution function (WDF) and the ambiguity function [6–12].

In one of these papers [11], the on-axis image irradiance is analyzed for varying focus errors and different types of primary aberrations using a two-dimensional WDF associated to a modified one-dimensional pupil function. However, in spite of being an interesting theoretical result, from a practical point of view the main shortcoming of this method is its lack of versatility due to the fact that the WDF must be recalculated for each different value of the aberration coefficients. Therefore, this approach is restricted only to the analysis of optical systems since in this case all the parameters are fixed. On the contrary synthesis involves a procedure in which at least one parameter of the system can be varied in order to get the optimum result.

The aim of this work is to generalize the result of Ref. [11]. This generalization is achieved mainly in two aspects. First, the intensity distribution can now be calculated not only on the optical axis but along arbitrary curves in the image space. These paths can be selected to obtain any desired partial feature of the whole tridimensional intensity distribution. The intensity along the curves is achieved from a single two-dimensional WDF display by adding the values of this representation along certain phase-space slices. The second aspect of the generalization points to the use of the method in a more efficient analysis (and also in the synthesis) of optical systems, since the spherical aberration coefficient and the defocus coefficient are both parameters that can be varied in order to achieve a particular irradiance distribution. In this case, a single WDF display serves to obtain the irradiance for a variable spherical aberration coefficient and defocus.

2. Basic theory

Let us consider an optical imaging system characterized by an arbitrary pupil mask $p(\xi,\eta)$, as sketched in Fig. 1. By using normalized polar coordinates

$$\xi = ar'\cos\theta', \quad \eta = ar'\sin\theta', \tag{1}$$

[1] Permanent address: Centro de Investigaciones Ópticas (CIOp), Casilla de Correo 124, (1900) La Plata, Argentina.

PII S0030-4018(97)00120-X

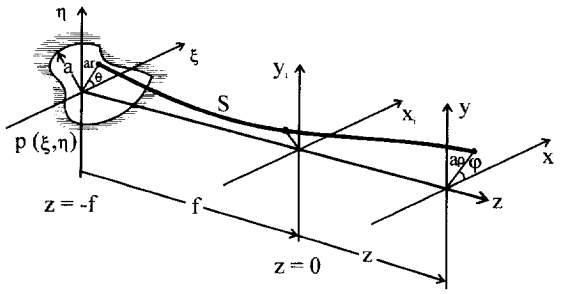

Fig. 1. A schematic illustration of an imaging optical system. The function $p(\xi,\eta)$ is the pupil with maximum height a; (x_i,y_i) are the coordinates at the image plane ($z=0$); (x,y) are the coordinates of a defocused plane. The line S represents a typical path in the image space.

the monochromatic field amplitude distribution at an arbitrary point $(x,y;z)$, in the image space, can be written as

$$U(x,y;z) = \frac{A}{\lambda(f+z)}\int_0^1\int_0^{2\pi} P(r',\theta') \times\exp\left[\frac{2\pi i}{\lambda}W(r',\theta';z)\right] \times\exp\left[-\frac{2\pi i a r'}{\lambda(f+z)} \times(x\cos\theta' + y\sin\theta')\right] r'\,dr'\,d\theta', \tag{2}$$

where A is the constant incident amplitude, and λ is the wavelength. $P(r',\theta')$ and $W(r',\theta')$ are the pupil function and the aberration function, respectively, in polar coordinates. The analysis of the irradiance in the image space is performed along curves which can be expressed in parametric form as $x(z)$ and $y(z)$, like the one depicted in Fig. 1. By employing polar coordinates

$$x(z) = a\rho(z)\cos\varphi(z), \quad y(z) = a\rho(z)\sin\varphi(z), \tag{3}$$

Eq. (2) can be rewritten as

$$U(\rho(z),\varphi(z);z) = \frac{A}{\lambda(f+z)}\int_0^1\int_0^{2\pi} P(r',\theta') \times\exp\left[\frac{2\pi i}{\lambda}W(r',\theta';z)\right] \times\exp\left[-\frac{2\pi i a^2 r'}{\lambda(f+z)}\rho(z) \times\cos(\theta'-\varphi(z))\right] r'\,dr'\,d\theta'. \tag{4}$$

Now, we perform the following transformation of the pupil function

$$P(r',\theta')\exp\left[\frac{2\pi i}{\lambda}W(r',\theta';z)\right] = Q(r',\theta')\exp\left(\frac{2\pi i}{\lambda}W_{20}r'^2\right)\exp\left(\frac{2\pi i}{\lambda}W_{40}r'^4\right), \tag{5}$$

i.e., we define a generalized pupil function $Q(r',\theta')$ as the product between the aperture transmittance $P(r',\theta')$ and the phase exponential that takes into account all the aberrations except from the defocus effect ($W_{20}r'^2$) and the spherical aberration ($W_{40}r'^4$) which are separately written in Eq. (5). The defocus coefficient W_{20} is given by

$$W_{20} = \frac{a^2 z}{2f(f+z)}. \tag{6}$$

By considering Eq. (5), Eq. (4) takes the form

$$U(\rho(z),\varphi(z);z) = \frac{A}{\lambda(f+z)}\int_0^1 F(r';\rho(z),\varphi(z)) \times\exp\left[\frac{2\pi i}{\lambda}\left(W_{20}r'^2 + W_{40}r'^4\right)\right] r'\,dr', \tag{7}$$

with

$$F(r';\rho(z),\varphi(z)) = \int_0^{2\pi} Q(r',\theta')\exp\left[-\frac{2\pi i a^2 r'}{\lambda(f+z)}\rho(z) \times\cos(\theta'-\varphi(z))\right] d\theta'. \tag{8}$$

The change of variable

$$r'^2 = \mu + \tfrac{1}{2}, \tag{9}$$

in Eq. (7) leads to the following result for the intensity distribution

$$I(\rho(z),\varphi(z);z) = |U(\rho(z),\varphi(z);z)|^2 = \frac{1}{4\lambda^2(f+z)^2}\int_{-\infty}^{+\infty}\int_{-\infty}^{+\infty} f_z(\mu)f_z^*(\mu') \times\exp\left\{\frac{2\pi i}{\lambda}\left[(W_{20}+W_{40})(\mu-\mu') + W_{40}(\mu^2-\mu'^2)\right]\right\} d\mu\,d\mu', \tag{10}$$

where

$$f_z(\mu) = \begin{cases} F(r';\rho(z),\varphi(z)), & -\tfrac{1}{2}\le\mu\le\tfrac{1}{2}, \\ 0, & \text{otherwise.} \end{cases} \tag{11}$$

By using the Wigner distribution function, which is a dual phase-space representation of a signal $f(x)$, defined as

$$W_f(x,\nu) = \int_{-\infty}^{+\infty} f\left(x+\frac{x'}{2}\right) f^*\left(x-\frac{x'}{2}\right) \times \exp(-2\pi i \nu x')\,dx', \quad (12)$$

Eq. (10) can be rewritten as

$$I(\rho(z),\varphi(z);z) = \frac{1}{4\lambda^2(f+z)^2} \times \int_{-\infty}^{+\infty}\int_{-\infty}^{+\infty} f_z\left(\zeta+\frac{\zeta'}{2}\right) f_z^*\left(\zeta-\frac{\zeta'}{2}\right) \times \exp\left\{\frac{2\pi i}{\lambda}\left[2\zeta W_{40} + (W_{20}+W_{40})\right]\zeta'\right\} d\zeta\, d\zeta' = \frac{1}{4\lambda^2(f+z)^2} \times \int_{-\infty}^{+\infty} W_{f_z}\left(\zeta, -\frac{2W_{40}}{\lambda}\zeta - \frac{W_{40}}{\lambda} - \frac{W_{20}}{\lambda}\right) d\zeta. \quad (13)$$

Therefore, the procedure to derive Eq. (13) can be summarized in the following steps. First, a generalized pupil function $Q(r',\theta')$ (in polar coordinates) is obtained from the amplitude transmittance $P(r',\theta')$ and from the wave-aberration function $W(r',\theta')$, as given in Eq. (5). Then, the angular integration (Eq. (8)) and the change of variable (Eq. (9)) are performed to achieve a one-dimensional modified pupil function $f_z(\mu)$ (see Eq. (11)). Next, the two-dimensional WDF of $f_z(\mu)$ is digitally obtained. It should be noted that for different paths in the image space $(\rho(z),\varphi(z))$, the function $f_z(\mu)$ changes accordingly with Eqs. (8)–(11). Finally, the irradiance along these paths can be found from the space-coordinate projection of the WDF associated with $f_z(\mu)$, along a straight line in the phase-space (x,ν) given by

$$\nu = -2\frac{W_{40}}{\lambda}x - \frac{W_{40}}{\lambda} - \frac{W_{20}}{\lambda}. \quad (14)$$

The versatility of the computation method becomes evident when one realizes that from a single phase-space distribution the values of the irradiance at a given point can be obtained for variable spherical aberration and defocus, since both are parameters in Eq. (13). Moreover, for certain paths the function $f_z(\mu)$ does not depend on the variable z and therefore, in these cases the values of the irradiance at every point in a given curve can be obtained from the same WDF. Furthermore, inspection of Eqs. (13) and (14) reveals that the wavelength is also a parameter. This result can be used in the calculation of quality parameters of systems working under polychromatic illumination. For the analysis of such systems it is necessary to compute the irradiance point by point for a large number of wavelengths, thus this approach is very well adapted to this situation. Next, we illustrate the performance of the method with some particular cases.

3. Examples

In the following examples we focus our attention on three particular paths in the image space which are depicted in Fig. 2, namely: optical axis, straight line passing through the center of the exit pupil with an arbitrary angle α (line A), and a straight line parallel to the optical axis (line B). A common feature of the irradiance along these lines is that in each case it can be obtained from a single two-dimensional Wigner representation of the function $F(r';\rho(z),\varphi(z))$ as it is shown in the following.

3.1. Optical axis

In this case $\rho(z) = 0$ for all values of z, and therefore

$$F(r',\rho(z)=0,\varphi) = \int_0^{2\pi} Q(r',\theta')\,d\theta' = 2\pi\tau_0(r'), \quad (15)$$

with $\tau_0(r')$ the angular average of the generalized pupil function $Q(r',\theta')$ at every value of r'. This result agrees with McCutchen's theorem [13] which, in this case, states that the irradiance axial behavior of the system only depends on the above average.

3.2. Straight line parallel to the optical axis

A straight line parallel to the optical axis is defined by $\rho(z) = \rho_0$, $\varphi(z) = \theta_0$, with (ρ_0,θ_0) being the normalized coordinates of the point of intersection between the straight line and the pupil plane. By considering $f \gg z$ (short paths around the focal plane), we found

$$F(r';z) = \int_0^{2\pi} Q(r',\theta') \times \exp\left(-\frac{2\pi i a^2 r'\rho_0}{\lambda f}\cos(\theta'-\theta_0)\right) d\theta', \quad (16)$$

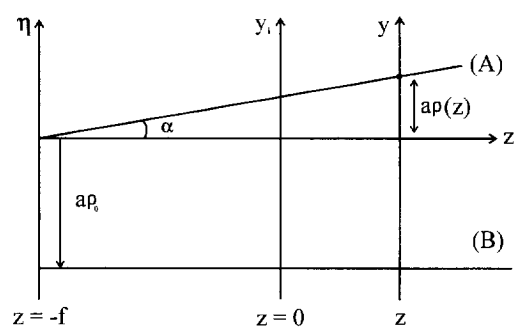

Fig. 2. Side view of the system in Fig. 1. The straight lines (A) and (B) and the optical axis z are the paths along which the analysis of the irradiance is performed in the examples in Sections 3.1, 3.2, and 3.3.

which is independent of z. In particular, if $Q(r',\theta') = Q(r')$, the result is separable in the form

$$F(r') = Q(r')\,2\pi J_0\left(\frac{2\pi a^2 r'\rho_0}{\lambda f}\right), \tag{17}$$

where J_0 is the Bessel function of first kind and order zero.

3.3. Straight line passing through the center of the exit pupil

In this case $\rho(z) = \tan(\alpha)(f+z)/a$, $\varphi(z) = \theta_0$, where α is the angle between the straight line and the optical axis (see Fig. 2). Thus, Eq. (8) results

$$F(r';z) = F(r') = \int_0^{2\pi} Q(r',\theta') \times \exp\left[-\frac{2\pi i a r'}{\lambda}\tan(\alpha)\cos(\theta' - \theta_0)\right] d\theta', \tag{18}$$

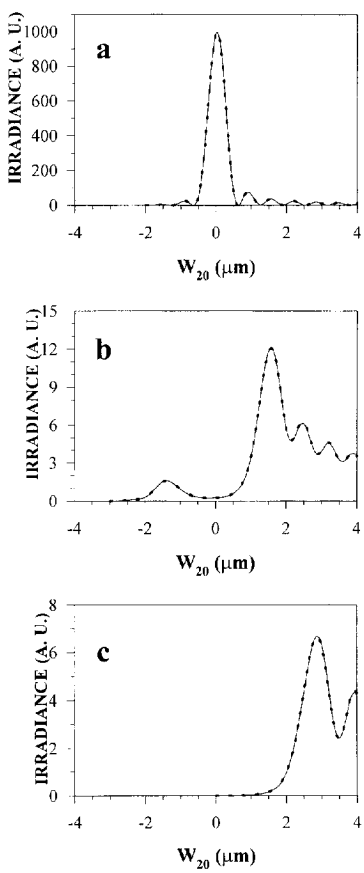

Fig. 3. Values of the irradiance as a function of the defocus coefficient defined by Eq. (6), obtained for a circular aperture with $W_{40} = 0$ along particular cases of the straight line (A) in Fig. 2: (a) optical axis, (b) $\alpha = 0.012°$, and (c) $\alpha = 0.024°$. The results are obtained with our proposal (continuous line) and with the method in Ref. [14] (dotted line).

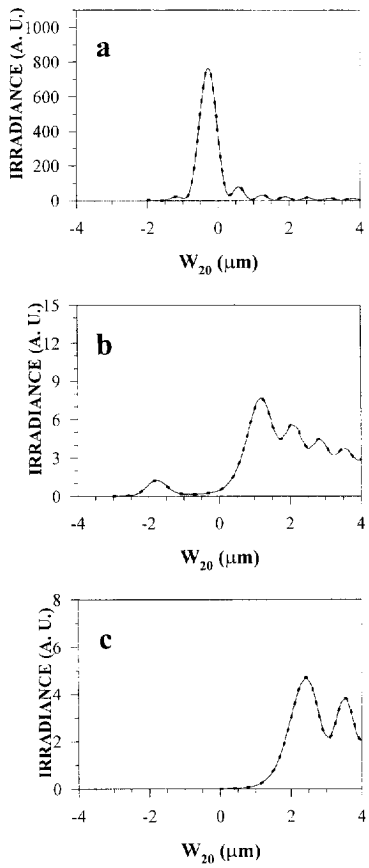

Fig. 4. Same as in Fig. 3 with $W_{40} = \lambda/2$.

which is also independent of z. If $Q(r',\theta') = Q(r')$, the result can be expressed as the product of the generalized pupil function and a zero order Bessel function; i.e.,

$$F(r') = Q(r')\,2\pi J_0\left(\frac{2\pi}{\lambda} a r' \tan\alpha\right). \tag{19}$$

4. Numerical simulations and discussion

In order to test the performance of our method, we computed the irradiance at 256 points along the straight lines defined in Section 3, for two different pupil functions illuminated with monochromatic light of wavelength $\lambda = 632.8$ nm. For the focal distance $f = 15.8$ m is assumed. The results are compared with those obtained by the method of Yzuel et al. [14] which is a classical numerical method for the calculation of diffraction patterns.

In the first case, we considered a circular aperture of 10 mm radius. The results assuming no spherical aberration and with $W_{40} = \lambda/2$ are shown in Figs. 3 and 4, respectively, for three axes passing through the center of the exit pupil with different inclinations with respect to the optical

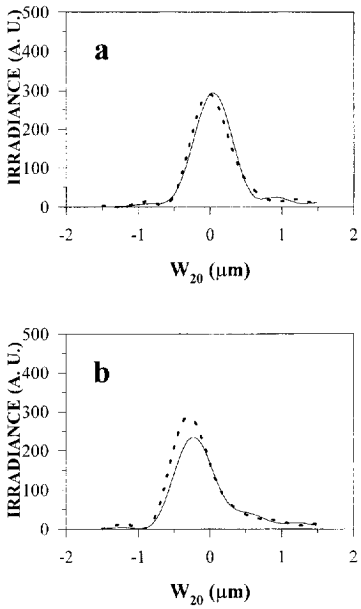

Fig. 5. Values of the irradiance obtained for a circular aperture along a straight line parallel to the optical axis at +0.33 mm from the origin (line (B) in Fig. 2): (a) $W_{40} = 0$ and (b) $W_{40} = \lambda/2$. The results are obtained with our proposal (continuous line) and with the method in Ref. [14] (dotted line).

axis. For a line parallel to the optical axis at 0.33 mm the results with and without spherical aberration are shown in Figs. 5(a) and 5(b).

A more general kind of pupil was considered in the next example. It consists of a circular aperture of 10 mm radius with a decentered circular obscuration, the ratio of the inner to outer radii being 1/3. For the calculation we assumed that the obscuration is tangent to the center of the pupil and that it is displaced towards the upper side in the vertical axis as sketched in Fig. 6.

The irradiance was calculated in the neighbourhood of

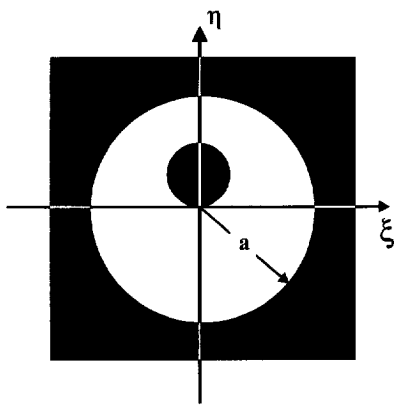

Fig. 6. Pupil function composed of a circular aperture with a circular decentered obscuration.

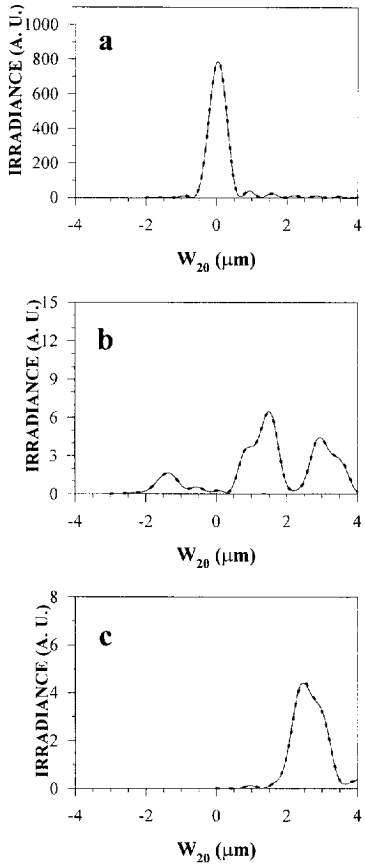

Fig. 7. Same as in Fig. 3 for the pupil function of Fig. 6.

the image plane along the same axes defined in the previous case. In all cases the inclination was taken in the same direction of the displaced obscuration (see the angle α in Fig. 2). Again we considered two cases $W_{40} = 0$ and $W_{40} = \lambda/2$. The corresponding results are plotted in Figs. 7 and 8, respectively. For this pupil function (with and without spherical aberration) we also computed the irradiance along a line parallel to the optical axis at +0.33 mm on the ζ axis; see Figs. 9(a) and 9(b).

The inspection of Figs. 3 to 5 and 7 to 9 shows that the results obtained with our method match very well with those achieved with the method of Yzuel et al. In Figs. 3, 4, 7 and 8 the results corresponding to both numerical methods are indistinguishable since their data points differ by less than 0.03%. The main differences can be appreciated in Figs. 5 and 9, from which can be inferred that the assumption $f \gg z$ in Section 3.2 is very severe and therefore, the accuracy of the results obtained with this approximation are acceptable only for points that lie very close to the image plane.

It should be noted that, in spite of that, in the preceding examples the Fresnel number of the systems are about

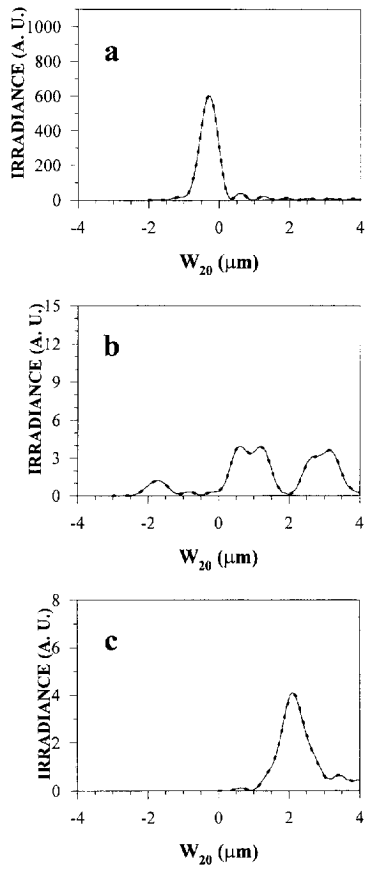

Fig. 8. Same as in Fig. 7, with $W_{40} = \lambda/2$.

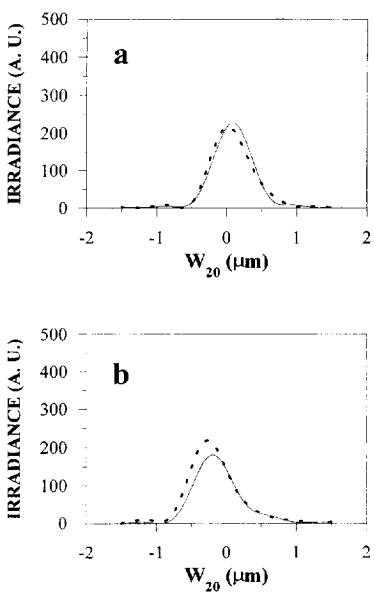

Fig. 9. Same as in Fig. 5, for the pupil function of Fig. 6.

$N = 10$, the method imposes no-restriction on the Fresnel number of the systems to be analyzed.

Summarizing, we have shown that the values of the irradiance along different paths in the image space can be obtained for variable spherical aberration and defocus from the WDF of a one-dimensional modified pupil function. We have discussed in detail certain interesting paths for which a single two-dimensional WDF allows one to obtain the whole set of irradiances. Furthermore, this method can be applied to other trajectories for which the approximations made in Section 3.2 also hold. We want to point out that the results obtained in the numerical simulations showed that our method is very efficient, since it drastically reduces the computation time, compared with the method in Ref. [14]. A more detailed comparative analysis between the present method and others available in the literature is the subject of future work.

Acknowledgements

This research was mainly supported by the Dirección General de Investigación Científica y Técnica (grant PB93-0354-C02-01), Spain. E. Silvestre gratefully acknowledges the financial support of this institution. E.E. Sicre carried out this research under contract CI1*CT93-0109 financed by the Commission of the European Communities (initiative Marie Curie fellowships).

References

[1] Lord Rayleigh, Philos. Mag. 8 (1879) 432.
[2] K. Strehl, Z. Instrumentenkd. 22 (1903) 213.
[3] A. Maréchal, Rev. d'Optique 26 (1947) 257.
[4] H.H. Hopkins, Proc. Phys. Soc. London B 70 (1957) 449.
[5] H.H. Hopkins, Optica Acta 13 (1966) 343.
[6] K.-H. Brenner, A.W. Lohmann, J. Ojeda-Castañeda, Optics Comm. 44 (1983) 323.
[7] H. Bartelt, J. Ojeda-Castañeda, E.E. Sicre, Appl. Optics 23 (1984) 2693.
[8] J. Ojeda-Castañeda, P. Andrés, E. Montes, J. Opt. Soc. Am. A 4 (1987) 313.
[9] L.V. Bourimborde, W.D. Furlan, E.E. Sicre, J. Mod. Optics 38 (1991) 1685.
[10] W.D. Furlan, G. Saavedra, J. Lancis, Optics Comm. 96 (1993) 208.
[11] D. Zalvidea, M. Lehman, S. Granieri, E.E. Sicre, Optics Comm. 118 (1995) 207.
[12] W.D. Furlan, G. Saavedra, E. Silvestre, M.J. Yzuel, P. Andrés, Proc. SPIE 2730 (1996) 252.
[13] C.W. McCutchen, J. Opt. Soc. Am. 54 (1964) 240.
[14] M.J. Yzuel, F. Calvo, Optica Acta 30 (1983) 233.